LETTER

doi:10.1038/nature11669

Quasi-cylindrical wave contribution in experiments on extraordinary optical transmission

Frerik van Beijnum[1], Chris Rétif[2], Chris B. Smiet[1], Haitao Liu[3], Philippe Lalanne[4] & Martin P. van Exter[1]

A metal film perforated by a regular array of subwavelength holes shows unexpectedly large transmission at particular wavelengths, a phenomenon known as the extraordinary optical transmission (EOT) of metal hole arrays[1]. EOT was first attributed to surface plasmon polaritons, stimulating a renewed interest in plasmonics[2–4] and metallic surfaces with subwavelength features[5–7]. Experiments soon revealed that the field diffracted at a hole or slit is not a surface plasmon polariton mode alone[8]. Further theoretical analysis[9] predicted that the extra contribution, from quasi-cylindrical waves[10–13], also affects EOT. Here we report the experimental demonstration of the relative importance of surface plasmon polaritons and quasi-cylindrical waves in EOT by considering hole arrays of different hole densities. From the measured transmission spectra, we determine microscopic scattering parameters which allow us to show that quasi-cylindrical waves affect EOT only for high densities, when the hole spacing is roughly one wavelength. Apart from providing a deeper understanding of EOT, the determination of microscopic scattering parameters from the measurement of macroscopic optical properties paves the way to novel design strategies.

Understanding EOT quantitatively has been one of the main challenges in plasmonics in the past decade (see ref. 7 for a review). An important contribution to EOT may be the quasi-cylindrical wave (QCW), which is the field diffracted at a subwavelength indentation on the metal surface, simultaneously with the surface plasmon polariton (SPP) contribution[10,11,13]. The justification for separating these two field contributions lies in the fact that QCWs exist in the absence of SPPs, that is, for a perfect electric conductor interface[10,12,14] and for a dielectric interface[15]. For a perfect electric conductor, the QCW is just a cylindrical wave in free space with a $1/x^{1/2}$ decay rate, x being the distance to the scatterer. For metals of finite conductivity at optical frequencies, the cylindrical-wave behaviour is seen only in the vicinity of the indentation, within a distance of a few wavelengths. Farther from the indentation, the QCW decay rate increases until it reaches an asymptotic algebraic value of $1/x^{3/2}$ at large distances ($x \to \infty$). Because of the periodicity of hole arrays, all these decay rates are simultaneously present in EOT.

Another important result in our understanding of EOT was the development of a semi-analytic SPP model, which quantifies the SPP contribution to EOT. This microscopic model relies on scattering parameters that describe the interaction between the incident light and the holes. The microscopic model correctly predicts the EOT line shape but underestimates the magnitude of the transmission by a factor of roughly two for visible frequencies. These results suggest that SPPs are responsible for only about 50% of EOT[9], with the other 50% due to QCWs. So far, this interpretation is purely theoretical and remains conceptual, and we are not aware of any experimental confirmation. The likely reason for this is that many scattering parameters in the model are dispersive and had to be calculated using complicated simulations[9]. Measuring all these parameters with sufficient accuracy is a tremendous experimental challenge that we address here.

In this Letter, we provide direct evidence for the respective roles of SPPs and QCWs in EOT, by exploiting the fact that they have different characteristic damping lengths. We do this by measuring the transmission spectra of a series of hole arrays with varying hole densities, designed to resonate at the same near-infrared frequency (~750 nm). We find that the normalized transmission peaks of all the low-density arrays are almost identical. The array of highest density, which corresponds to the classical hole array in ref. 1, has a hole spacing that corresponds to a QCW damping length of one wavelength. This array shows a pronounced increase in normalized transmission compared with the transmission of the other arrays. The observation of this atypical behaviour for the highest-density array is direct proof of the involvement of QCWs in EOT, or more generally of the QCWs in phenomena related to subwavelength metallic gratings.

Figure 1a illustrates how we vary the hole density: we increase the distance between 'hole chains' (lines of holes whose separation in the y direction, $a_y = a_0 = 450$ nm, we do not vary) while keeping the properties of these chains fixed. The distance between the chains is chosen to be $a_x = qa_0$, where $q = 1$, 2, 3, 4, 6 and 7. The holes perforate two metal layers: a 150-nm gold layer that is deposited on a glass substrate, and a 20-nm chrome layer that damps the SPP at the air interface (Fig. 1b). Figure 1c shows a scanning electron microscope image of the $q = 2$ hole array. We measure the zeroth-order transmission spectra of each array using light polarized in the x direction. As a result, SPPs propagating along the y axis are negligible[9,16–18].

Figure 2a shows the measured spectra on a semi-log scale. Each array has a transmission peak between 735 and 775 nm, which shifts to shorter wavelengths as the hole spacing increases. The transmission minima of these resonances are at 724 ± 4 nm, which is very close to 729 nm, the expected value of $\mathrm{Re}(n_{\mathrm{eff}})a_0$, where n_{eff} is the ratio between the magnitude of the SPP wavevector and that of the free-space wavevector[19,20]. The magnitudes of the transmission minima range between 0.6×10^{-4} and 2×10^{-4}. The resonance peaks are the result of a surface wave propagating in the x direction, with the number of oscillations per lattice period equal to the value of q for the hole array. For $q = 4$, 6 and 7, additional resonances are also visible at wavelengths between 800 and 1,000 nm. These resonances correspond to a surface wave propagating in the x direction with $q - 1$ oscillations per period.

As evidenced by the log-scale plots, the zeroth-order transmission drastically decreases as the hole density decreases. As will be explained below (equation (2)), it essentially scales as $1/q^2$. Thus, in Fig. 2b we plot the product of q^2 and transmission on a linear scale, for $q = 1$, 2, 4 and 6. The results for $q = 3$ and 7 have been removed for clarity. By plotting the data on a linear scale, we see that the scaled transmission is almost constant when going from $q = 2$ to $q = 6$. However, for $q = 1$ the transmission peak is markedly larger, being more than two times larger than all the other peaks. The fact that all the arrays except $q = 1$ have almost identical extraordinary transmission peaks is not coincidental and, as will be explained below, reveals the resonant transmission due to SPPs only. In this respect, the sudden and marked

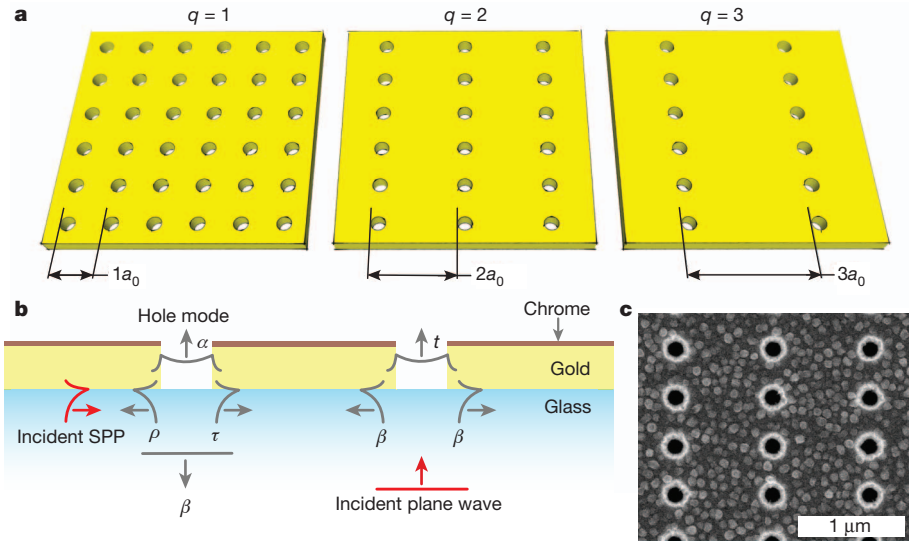

Figure 1 | Sample design. To demonstrate a QCW contribution to EOT, we compare the transmissions of a series of hole arrays that have different densities and all resonate at the same wavelength. **a**, To decrease the hole density, the distance between hole chains is increased. **b**, The relevant scattering processes. At the left hole chain, there is an incident SPP (red arrow) that is transmitted (τ), reflected (ρ), coupled into the hole (α) or coupled to free space (β). At the right hole chain, there is an incident free-space mode (red arrow) that scatters into a SPP (β) or couples into the hole (t). **c**, Scanning electron microscope picture of the $q = 2$ hole array.

increase of the peak transmission for the highest density ($q = 1$) is one of our main results: it is a direct signature of the additional short-range contribution of the QCWs to EOT.

The previous conclusion is inferred qualitatively on the basis of the difference in damping lengths between SPPs and QCWs. Using the microscopic SPP model in ref. 9, we now aim at providing a fully quantitative analysis of the data in Fig. 2 to support our conclusions explicitly. The main drawback of the microscopic approach is that it requires knowledge of many dispersive, complex-valued parameters, which need to be calculated using full-vectorial simulations at every wavelength. This precludes its direct application to the analysis of experimental data. Below we discuss the model in depth and show that an analytical expression involving only five independent, real, non-dispersive, fitted parameters accurately reproduces the whole set of experimental spectra in Fig. 2 for $q \geq 2$, but produces wrong predictions for $q = 1$.

The microscopic model, as originally formulated in ref. 9, considers one-dimensional hole chains (along the y direction) to be the elementary scatterers of the hole arrays and assumes that the electromagnetic interaction between the hole chains is mediated only by the SPP modes on unperturbed interfaces, the QCWs being totally neglected. The microscopic model couples three modes: the SPP mode at the gold–glass interface, which consists of SPPs propagating in both directions along the x axis; the fundamental mode within the holes; and the free-space modes.

The modes are coupled by the following scattering parameters (Fig. 1b). An incident SPP can couple into the holes of the hole chain (α), couple to free space (β), or be transmitted (τ) or reflected (ρ). An incident plane wave can couple to a SPP (β) or directly into the holes of the hole chain (t). The propagation of the SPP from one hole chain to another is described by $e^{-ik_{spp}a}$, where $k_{spp} = 2\pi n_{eff}/\lambda$ is the wavevector magnitude of the SPP on a flat gold–glass interface and a is the distance between the hole chains. Because we keep the hole size constant for each array, the scattering parameters (α, β, ρ, τ and t) should be the same for each array. Only the hole spacing a_x depends on the parameter q: $a_x = qa_0$.

In line with the coupled-mode approach proposed in ref. 9, we derive (Supplementary Information) the transmission coefficient, t_f, of a single hole chain, modified by the SPPs excited at the surrounding hole chains:

$$t_f = t + \frac{2\alpha\beta}{e^{-ik_{spp}a} - (\rho + \tau)} \tag{1}$$

The assumption that the hole chains excite only a plane SPP wave in the x direction is valid if the incident polarization is along the x axis. Moreover, the holes within the hole chain have to be less than a SPP wavelength apart[9]. The model neglects the influence of the metal–air interface. In Supplementary Information, we show that this assumption holds if the SPPs at that interface are sufficiently damped by the chrome layer.

The optical transmission measured at a particular angle is a sum of the field contributions from all illuminated hole chains. If we define N_0 as the number of illuminated hole chains for the $q = 1$ array, $N = N_0/q$ is the number of hole chains as a function of q. In the zeroth diffraction order, the contributions from all hole chains are in phase, and the transmitted intensity is hence[21]

$$T \propto 1/q^2 |t_f|^2 \tag{2}$$

where the proportionality factor is independent of q (Supplementary Information).

Equations (1) and (2) are not yet simple enough to be used to model experimental data. The six scattering parameters are complex, such that there are twelve real-valued parameters. To reduce the number of free parameters, we combine α and β into $\alpha\beta$ and ρ and τ into $\rho + \tau$. Furthermore, we need only consider the phase difference between t and $\alpha\beta$. For the complex variable k_{spp}, we combine previously measured, linearly interpolated values for the gold properties[22] with a measured value of the index of refraction of the substrate (1.51). This leaves us with a model with five free parameters.

Another crucial step towards fitting the model to the data is the wavelength dependence of the parameters. We use the following approximations: $t \propto \lambda^{-2}$, as indicated by several studies[7,23–25]; $\alpha\beta \propto \lambda^{-4}$, in rough agreement with fourfold reduction in the magnitude of $\alpha\beta$ for a wavelength increase of 38% (ref. 9); we keep $\rho + \tau$ constant, as calculations show that this sum has limited dispersion; the phase of $\rho + \tau$ and the phase difference between $\alpha\beta$ and t are also kept constant as functions of wavelength. As a result, we have the following fit equation:

$$T = q^{-2} \left| \frac{\lambda_0^2}{\lambda^2} p_1 + \frac{\lambda_0^4}{\lambda^4} \frac{p_2 e^{ip_3}}{e^{-ik_{spp}qa_0} - p_4 e^{ip_5}} \right|^2 \tag{3}$$

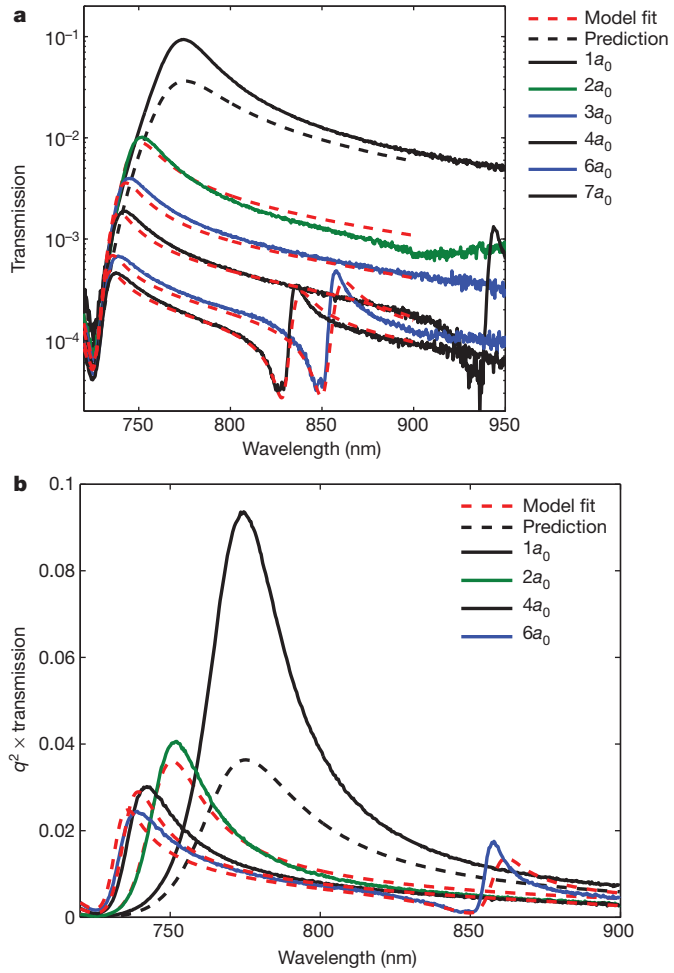

Figure 2 | Measured transmission spectra (solid curves) and the fitted SPP model (red dashed curves). Each dashed curve has the same parameters except for the q value. The parameters are based on a fit of equation (3) to the data of arrays with $q \geq 2$. The black dashed curve is a model prediction, plotting equation (3) with the same parameters as the other curves but with $q = 1$. **a**, The model accurately predicts all maxima and minima of the measured data for $q \geq 2$, showing that the transmission of these arrays is dominated by SPPs. **b**, Plotting the product of q^2 and transmission shows that there is a marked increase in transmission for $q = 1$ relative to the other arrays. By also plotting the SPP model, we show that this behaviour is not predicted by considering SPPs alone.

where $\lambda_0 = 800$ nm and p_1 to p_5 are the five real-valued parameters in the model. The physical significance of parameters p_1 and p_4 is discussed in Supplementary Information.

The fitted curves obtained with the model are shown with the red dashed curves in Fig. 2. For the fit, we only used the data of arrays $q = 2$ to $q = 7$, as we expect the transmission of these arrays to be dominated by SPPs. To ensure that the minima are fitted well, we fitted the base-10 log of the model to that of the data. The result is plotted in Fig. 2a, and the fit values are given in Table 1. For the arrays with $q = 2$, 3, 4, 6 and 7, the model describes the spectral positions of all minima and maxima very accurately, including the $(q - 1, 0)$ resonances that appear close to the wavelength of 850 nm. The transmission magnitude also is well modelled.

Notably, equation (3) (Fig. 2, dashed black curves) fails to predict the experimental data for $q = 1$. In particular, it underestimates the transmission peak by a factor of 2.5. The latter is consistent with the theoretical predictions in ref. 9, which conclude that SPPs account for only half of the total transmitted energy at peak transmittance for a resonance wavelength of 700 nm. In Supplementary Information, we expand the SPP microscopic model to incorporate QCWs (see equation (4) therein), and this extended model accurately describes the experimental data for $q = 1$ (Supplementary Fig. 3). We emphasize that this result is achieved using the same scattering parameters and does not require any additional fitting.

Table 1 | The values of the fitting parameters p_1 to p_5

Parameter	Fit value	Error
p_1	0.0740	0.0006
p_2	0.0243	0.0006
p_3	0.681π	0.013π
p_4	0.857	0.009
p_5	0.132π	0.006π
$\lvert\exp(-ik_{spp}a_0)\rvert$	1.021	NA

For completeness, we also give the value of $\lvert\exp(-ik_{spp}a_0)\rvert$, evaluated at 800 nm. We also give an estimate of the error in the fit values. NA, not applicable.

The observation that the transmission spectra of these six different hole arrays (including the particular $q = 1$ case) can be described with only five parameters is a considerable success of the microscopic theory. Moreover, it is of importance that these parameters are directly related to elementary scattering processes. It seems that the resonance of a perforated metal surface can be modelled with a combination of an SPP mode and a QCW on an unperturbed surface, taking into account a few extra scattering parameters, which can be inferred from simple transmission measurements.

Our experiments quantitatively show the respective contributions of SPPs and QCWs to EOT. The main step in our analysis was the derivation of the elementary scattering parameters defined in ref. 9 from classical transmission measurements performed on a series of hole arrays. The possibility of making these microscopic scattering parameters experimentally accessible may be paramount in understanding and designing complex periodic or aperiodic metallic structures. Hence, variations on this modelling approach may have important implications in applying plasmonic structures to sensors, photovoltaics, light-emitting diodes and lasers.

METHODS SUMMARY

The sample was fabricated as follows. Using electron-beam lithography, we created pillars on a glass substrate. Then we deposited 150 nm of gold and, subsequently, 20 nm of chrome. Finally, we etched away the pillars. Using scanning electron microscope pictures of each array, we measured the average hole radius to be 81 ± 4 nm. By studying the position of the diffraction orders using a 635-nm laser diode, we found that for all arrays a_0 has the same value to within 2 nm. Each array covers an area of 400 μm × 400μm.

The transmission spectra were measured using the following set-up. The light of a halogen lamp was filtered (long pass, 600 nm) and coupled to a 200-μm-diameter fibre. The light coupled out of the fibre was polarized along the x axis. The end facet of the fibre was imaged onto the sample with a magnification of 1.5. The 300-μm-diameter spot was centred on the 400 μm × 400 μm arrays. The zeroth-order transmission was imaged (magnification, 2/3) onto a 365-μm-diameter fibre that led to an Ocean Optics 2000+ USB spectrometer. To measure the reference spectrum, we moved the sample out of the beam using a stage.

An accurate measurement of the transmission spectrum requires sufficient spatial and temporal coherence of the illuminating and detected light. The spatial coherence at the sample was guaranteed by the limited numerical aperture $(\sim(6 \pm 2) \times 10^{-3})$ of the illumination. This corresponded to a coherence length of a few tens of micrometres on the sample[21], which is much longer than an SPP propagation length. Temporal coherence was ensured by the spectral resolution of the detecting spectrometer. The 1-nm resolution corresponded to coherence times of hundreds of femtoseconds[21] and was an order of magnitude finer than strictly needed.

Received 6 June; accepted 4 October 2012.

1. Ebbesen, T. W., Lezec, H. J., Ghaemi, H. F., Thio, T. & Wolff, P. A. Extraordinary optical transmission through sub-wavelength hole arrays. *Nature* **391,** 667–669 (1998).
2. Yanik, A. A. *et al.* An optofluidic nanoplasmonic biosensor for direct detection of live viruses from biological media. *Nano Lett.* **10,** 4962–4969 (2010).
3. Oulton, R. F. *et al.* Plasmon lasers at deep subwavelength scale. *Nature* **461,** 629–632 (2009).
4. Atwater, H. A. & Polman, A. Plasmonics for improved photovoltaic devices. *Nature Mater.* **9,** 205–213 (2010).

5. Barnes, W. L., Dereux, A. & Ebbesen, T. W. Surface plasmon subwavelength optics. *Nature* **424,** 824–830 (2003).
6. García de Abajo, F. J. Light scattering by particle and hole arrays. *Rev. Mod. Phys.* **79,** 1267–1290 (2007).
7. García-Vidal, F. J., Martín-Moreno, L., Ebbesen, T. W. & Kuipers, L. Light passing through subwavelength apertures. *Rev. Mod. Phys.* **82,** 729–787 (2010).
8. Gay, G. *et al.* The optical response of nanostructured surfaces and the composite diffracted evanescent wave model. *Nature Phys.* **2,** 262–267 (2006).
9. Liu, H. T. & Lalanne, P. Microscopic theory of the extraordinary optical transmission. *Nature* **452,** 728–731 (2008).
10. Lalanne, P. & Hugonin, J. P. Interaction between optical nano-objects at metallo-dielectric interfaces. *Nature Phys.* **2,** 551–556 (2006).
11. Dai, W. & Soukoulis, C. M. Theoretical analysis of the surface wave along a metal-dielectric interface. *Phys. Rev. B* **80,** 155407 (2009).
12. Lalanne, P., Hugonin, J. P., Liu, H. T. & Wang, B. A microscopic view of the electromagnetic properties of sub-λ metallic surfaces. *Surf. Sci. Rep.* **64,** 453–469 (2009).
13. Nikitin, A. Y., García-Vidal, F. J. & Martín-Moreno, L. Surface electromagnetic field radiated by a subwavelength hole in a metal film. *Phys. Rev. Lett.* **105,** 073902 (2010).
14. Nikitin, A., Yu, Rodrigo, S. G., García-Vidal, F. J. & Martín-Moreno, L. In the diffraction shadow: Norton waves versus surface plasmon polaritons in the optical region. *N. J. Phys.* **11,** 123020 (2009).
15. Gan, C. H., Lalouat, L., Lalanne, P. & Aigouy, L. Optical quasicylindrical waves at dielectric interfaces. *Phys. Rev. B* **83,** 085422 (2011).
16. Barnes, W. L., Murray, W. A., Dintinger, J., Devaux, E. & Ebbesen, T. W. Surface plasmon polaritons and their role in the enhanced transmission of light through periodic arrays of subwavelength holes in a metal film. *Phys. Rev. Lett.* **92,** 107401 (2004).
17. Stolwijk, D. *et al.* Enhanced coupling of plasmons in hole arrays with periodic dielectric antennas. *Opt. Lett.* **33,** 363–365 (2008).
18. Yin, L. *et al.* Subwavelength focusing and guiding of surface plasmons. *Nano Lett.* **5,** 1399–1402 (2005).
19. Lalanne, P., Sauvan, C., Hugonin, J. P., Rodier, J. C. & Chavel, P. Perturbative approach for surface plasmon effects on flat interfaces periodically corrugated by subwavelength apertures. *Phys. Rev. B* **68,** 125404 (2003).
20. Maystre, D., Fehrembach, A.-L. & Popov, E. Plasmonic antiresonance through subwavelength hole arrays. *J. Opt. Soc. Am. A* **28,** 342–355 (2011).
21. Born, M. & Wolf, E. *Principles of Optics* (Pergamon, 1986).
22. Palik, E. D. *Handbook of Optical Constants of Solids* 286–295 (Academic, 1985).
23. Bethe, H. A. Theory of diffraction by small holes. *Phys. Rev.* **66,** 163–182 (1944).
24. van der Molen, K. L. *et al.* Role of shape and localized resonances in extraordinary transmission through periodic arrays of subwavelength holes: experiment and theory. *Phys. Rev. B* **72,** 045421 (2005).
25. van Beijnum, F., Rétif, C., Smiet, C. B. & van Exter, M. P. Transmission processes in random patterns of subwavelength holes. *Opt. Lett.* **36,** 3666–3668 (2011).

Supplementary Information is available in the online version of the paper.

Acknowledgements We acknowledge E. R. Eliel for discussions. H.L. acknowledges a Poste Rouge fellowship from CNRS and the 973 Program (2013CB328701). This work is part of the research program of the Foundation for Fundamental Research on Matter (FOM), which is part of the Netherlands Organisation for Scientific Research (NWO).

Author Contributions F.v.B. was the primary researcher on the project; he designed the experiment and wrote the paper. With C.B.S., F.v.B. conducted the experiments and analysed the data. C.R. made the samples. H.L., P.L. and M.P.v.E. made essential contributions to interpreting the results and writing the manuscript.

Author Information Reprints and permissions information is available at www.nature.com/reprints. The authors declare no competing financial interests. Readers are welcome to comment on the online version of the paper. Correspondence and requests for materials should be addressed to F.v.B. (beijnum@physics.leidenuniv.nl).